JOURNAL OF THE AMERICAN COLLEGE OF CARDIOLOGY
VOL. 65, NO. 19, 2015

ISSN 0735-1097/$36.00
PUBLISHED BY ELSEVIER INC.
http://dx.doi.org/10.1016/j.jacc.2015.03.520

ORIGINAL INVESTIGATIONS

Interacting Resident Epicardium-Derived Fibroblasts and Recruited Bone Marrow Cells Form Myocardial Infarction Scar

Adrián Ruiz-Villalba, PhD,*† Ana M. Simón, PhD,‡ Cristina Pogontke, MSc,*§ María I. Castillo, MSc,*§ Gloria Abizanda, MSc,‡ Beatriz Pelacho, PhD,‖ Rebeca Sánchez-Domínguez, PhD,¶# José C. Segovia, PhD,¶# Felipe Prósper, MD, PhD,‡ José M. Pérez-Pomares, PhD*§

ABSTRACT

BACKGROUND Although efforts continue to find new therapies to regenerate infarcted heart tissue, knowledge of the cellular and molecular mechanisms involved remains poor.

OBJECTIVES This study sought to identify the origin of cardiac fibroblasts (CFs) in the infarcted heart to better understand the pathophysiology of ventricular remodeling following myocardial infarction (MI).

METHODS Permanent genetic tracing of epicardium-derived cell (EPDC) and bone marrow–derived blood cell (BMC) lineages was established using Cre/LoxP technology. In vivo gene and protein expression studies, as well as in vitro cell culture assays, were developed to characterize EPDC and BMC interaction and properties.

RESULTS EPDCs, which colonize the cardiac interstitium during embryogenesis, massively differentiate into CFs after MI. This response is disease-specific, because angiotensin II–induced pressure overload does not trigger significant EPDC fibroblastic differentiation. The expansion of epicardial-derived CFs follows BMC infiltration into the infarct site; the number of EPDCs equals that of BMCs 1 week post-infarction. BMC-EPDC interaction leads to cell polarization, packing, massive collagen deposition, and scar formation. Moreover, epicardium-derived CFs display stromal properties with respect to BMCs, contributing to the sustained recruitment of circulating cells to the damaged zone and the cardiac persistence of hematopoietic progenitors/stem cells after MI.

CONCLUSIONS EPDCs, but not BMCs, are the main origin of CFs in the ischemic heart. Adult resident EPDC contribution to the CF compartment is time- and disease-dependent. Our findings are relevant to the understanding of post-MI ventricular remodeling and may contribute to the development of new therapies to treat this disease. (J Am Coll Cardiol 2015;65:2057–66) © 2015 by the American College of Cardiology Foundation.

From the *Department of Animal Biology, Faculty of Sciences, University of Málaga, Málaga, Spain; †Department of Anatomy, Embryology and Physiology, AMC-University of Amsterdam, Amsterdam, the Netherlands; ‡Department of Hematology, Clínica Universitaria de Navarra-CIMA, Universidad de Navarra, Pamplona, Spain; §Andalusian Center for Nanomedicine and Biotechnology, Campanillas (Málaga), Spain; ‖Stem Cell Therapy Area, Foundation for Applied Medical Research, University of Navarra, Pamplona, Spain; ¶Differentiation and Cytometry Unit, Hematopoietic Innovative Therapies Division, Centro de Investigaciones Energéticas, Medioambientales y Tecnológicas-Centro de Investigaciones Biomédicas en Red de Enfermedades Raras, Madrid, Spain; and the #Advanced Therapies Mixed Unit, Instituto de Investigación Sanitaria-Fundación Jiménez Díaz, Madrid, Spain. Dr. Pelacho is supported by ISCIII PI13/02144 and CP09/00333. Dr. Segovia is supported by ISCIII RD12/0019-0023. Dr. Prósper is supported by ISCIII RD12/0019-0032. Dr. Pérez-Pomares is supported by MINECO grant BFU2012-35799, ISCIII RD12/0019-0022, Junta de Andalucía CTS-7564, and EU FP7-Marie Curie-ITN actions PITN-GA-2011-289600. All other authors have reported that they have no relationships relevant to the contents of this paper to disclose.

Manuscript received November 8, 2014; revised manuscript received February 4, 2015, accepted March 9, 2015.

ABBREVIATIONS AND ACRONYMS

BMC = bone marrow–derived cell

BZ = border zone

CD = cluster of differentiation

CF = cardiac fibroblast

EPDC = epicardium-derived cell

eYFP = enhanced yellow fluorescent protein

FACS = fluorescence-activated cell sorting

IZ = infarct zone

LT-HSC = long-term hematopoietic stem cell

MI = myocardial infarction

mRFP = monomeric red fluorescent protein

RZ = remote zone

SDF = stromal cell-derived factor

SMA = smooth muscle actin

Affecting millions of people, myocardial infarction (MI) is a leading cause of morbidity and mortality worldwide (1). Given increasing pressure to find clinical alternatives to heart transplantation, which is the only effective treatment for terminal cardiac failure that often results from MI, multiple researchers have sought to find an optimal cellular source to substitute dead or damaged cardiomyocytes with new, functional ones (2). However, knowledge of the cellular and molecular mechanisms that instruct and contribute to the normal, physiological repair of the injured heart remains very limited. This is paradoxical, because any experimental cell addition to the injured heart will eventually interact with endogenous cardiac reparative phenomena. Therefore, understanding such events is necessary to identify an optimal time point to inject cells with therapeutic properties into the damaged organ, and to critically analyze the poor results so far reported by cell infusion–based clinical trials attempting to fix the infarcted heart (3).

SEE PAGE 2067

During an MI, cardiac muscle death triggers an acute inflammatory response, led by circulating, bone marrow–derived blood cells (BMCs), which is followed by the mobilization of cardiac fibroblasts (CFs) in the ischemic region (4,5). After an MI, activated CFs expand to repair the injured area and deposit large amounts of extracellular matrix components, mainly collagen (6,7). This excessive deposition soon transforms into a growing scar; this disrupts the kinetic properties of the myocardial walls, impairing the mechanoelectric coupling of cardiomyocytes, increasing the risk of arrhythmias (8,9), and eventually leading to heart failure.

Despite the enormous clinical relevance of CFs, not much is known about their origin and biological properties in the context of ischemic heart disease. Interestingly, it has been suggested that characterizing CF biology in relation to the cells' origin could be instrumental in defining its genetic background and potential response to normal and pathologic conditions (10). Therefore, we aimed to identify the origin of CFs in the infarcted heart and study their interaction with BMCs during fibrotic ventricular remodeling.

METHODS

All animals used in this study were handled in compliance with institutional and European Union guidelines for animal care and welfare under a specific experimental procedure approved by the Ethics Committee of the University of Málaga. Homozygote *Wt1/IRES/GFP-Cre* (*Wt1*Cre) mice ($Cre^{+}/^{+}$) were crossed with *B6.129X1-Gt(ROSA)26Sortm1(EYFP)Cos/J* mice (Rosa26R-eYFP, The Jackson Laboratory, Bay Harbor, Maine). Wilm's Tumor Gene 1 (Wt1)-driven Cre activity mediates the excision of the LoxP-flanked STOP sequence in R26R mice, activating permanent reporter enhanced yellow fluorescent protein ($eYFP^{+}$) expression in the $Wt1^{+}$ cell lineage ($Wt1Cre\text{-}YFP^{+}$). Routine tissue extraction, fixation, and immunohistochemistry were performed as detailed in the Online Appendix (antibodies used are listed in Online Tables 1 and 2).

*Wt1*Cre-$eYFP^{+}$ nonmyocardial cell suspensions were washed in phosphate-buffered saline, and incubated in 2% fetal bovine serum and 10 mM 4-(2-hydroxyethyl)-1-piperazineethanesulfonic acid with the proper fluorochrome-conjugated primary immunoglobulin Gs (Online Table 3). Cell suspensions were analyzed in a MoFlo cell sorter (DakoCytomation, Glostrup, Denmark).

For bone marrow transplantations, 12-week to 16-week-old C57/BL and *Wt1*Cre-$eYFP^{+}$ host mice were irradiated and transplanted with bone marrow cells collected from monomeric red fluorescent protein (mRFP) donor mice, allowing for the full reconstitution of the hematopoietic system of recipient mice with constitutive mRFP-expressing cells. One and 3 months after transplantation the hematopoietic engraftment was analyzed by flow cytometry from peripheral blood samples via the analysis of mRFP fluorescence and antibodies against cluster of differentiation (CD) 45.1/CD45.2 pan-leucocyte isoforms (BD Biosciences, San Jose, California).

MI was induced by ligation of the left anterior descending coronary artery of 20- to 24-week-old mice as described elsewhere (11). Routine Mallory trichrome staining was performed to evaluate fibrosis, and samples were processed for immunohistochemistry and eYFP/mRFP visualization as previously mentioned.

Total ribonucleic acid from $eYFP^{+}/CD31^{-}$ cells sorted from dissected sham, remote, and infarcted zones was extracted using Tri-Reagent (Life Technologies, Grand Island, New York) and polymerase chain reaction performed in an Eco thermocycler (Illumina Inc., San Diego, California) as indicated in the Online Appendix.

Stromal cell–derived factor (SDF)-1α (R&D Systems, Minneapolis, Minnesota, 0.1 μg/ml in Hank's Balanced Salt Solution, Life Technologies, Thermo Fisher

Scientific Inc., Waltham, Massachusetts) was delivered to the ventricular walls of dissected *Wt1*Cre-eYFP$^+$ hearts by grafting SDF-1-embedded heparin-coated acrylic beads (100 to 300 μm in diameter) into the myocardium. Control beads were embedded in Hank's Balanced Salt Solution. Hearts were cultured for 8 hours in Dulbecco's modified Eagle medium (Life Technologies) and penicillin/streptomycin (37°C; 5% CO_2), washed in phosphate-buffered saline, and fixed in fresh 4% paraformaldehyde. All samples were counterstained with 4′,6-diamidino-2-phenylindole before eYFP inspection in an SP5 laser confocal microscope (Leica Microsystems, Buffalo Grove, Illinois).

For additional details on the experimental procedures, please refer to the Online Appendix.

RESULTS

The *Wt1*Cre-eYFP$^+$ offspring displayed permanent YFP reporter expression in the Wt1$^+$ cell lineage (from here onward referred to as eYFP$^+$; **Figure 1A**). At embryonic days (E) 10.0 to 11.5, eYFP$^+$ cells formed the epicardial epithelium (**Figures 1B to 1D**). Epicardial cell hypertrophy and generation of basal filopodia/lamellipodia indicated that the epithelial to mesenchymal transition that gives rise to epicardium-derived cells (EPDCs) (12-14) was active during this embryonic period (**Figures 1C and 1D**), but not at later fetal, perinatal, or adult stages. After E11.5, mesenchymal eYFP$^+$ EPDCs invaded the ventricular walls and occupied the nascent space between myocardial fibers, becoming the first cells colonizing the cardiac interstitium (**Figures 1D to 1F**). EPDC interstitial homing was completed between E15.5 and birth; eYFP$^+$ EPDCs remained conspicuous in the postnatal interstitium (**Figures 1E to 1H**).

Three eYFP$^+$ EPDC subtypes can be identified. The first one associated to coronary endothelium (eYFP$^+$/CD31$^+$/smooth muscle actin, type α [α-SMA$^-$], **Figures 1I and 1K**), and the second one to coronary smooth muscle (eYFP$^+$/CD31$^-$/α-SMA$^+$, **Figures 1J and 1K''**). The third type of EPDC (eYFP$^+$/PECAM1$^-$/α-SMA$^{low/-}$) displayed a characteristic spindle-shaped morphology and homes at the cardiac interstitium (**Figures 1K and 1K'**). These cells did not express significant amounts of fibroblast markers, such as collagen I (**Figure 1K''**), Fsp1, or Ddr2 (Online Figures 1A and 1B). To further characterize EPDC contribution to the cardiac interstitium, nonmyocardial cells from neonatal hearts were isolated and analyzed by fluorescence-activated cell sorting (FACS). eYFP$^+$ cells were 6.2 ± 1.3% of the total nonmyocardial cell pool, including 37.4 ± 5.1% of CD31$^+$ endocardial/coronary endothelial cells (**Figures 1L and 1M**). One-half (51.1 ± 4.9%) of eYFP$^+$ interstitial EPDCs were endocardial/coronary endothelial cells (CD31$^+$), whereas only 22.6 ± 3.5% of the nonendothelial (CD31$^-$) eYFP$^+$ cell fraction expressed the fibroblast and mesenchymal stem cell-related antigen CD90 (**Figure 1M'**) (15).

Because circulating BMCs have also been suggested to differentiate into CFs (10,16), the pan-leukocyte marker CD45 (17) was used to characterize BMC contribution to the embryonic cardiac interstitium. BMCs were rare in the early (E11.5 to E15.5) heart walls (Online Figures 2A to 2E′), but their numbers progressively increased from E15.5 to perinatal stages. Cardiac CD45$^+$ cells retained a circulating phenotype (**Figure 1N**), although some of them infiltrated the cardiac interstitium of cardiac chambers and acquired a fusiform phenotype (**Figure 1N'**). This late incorporation of blood-borne cells into the embryonic cardiac interstitium was confirmed by parabiotic experiments in avian embryos (Online Figures 2F to 2M′).

After birth, BMC cardiac homing was traced via mRFP$^+$ bone marrow transplantation to wild-type recipient mice. Two months after transplantation, BMC contribution to the healthy adult cardiac interstitium was low, but persistent (1.9 ± 0.6% of nonmyocardial cells; **Figures 1M and 1O**). Noncirculating, fusiform interstitial BMCs were CD45$^+$ (**Figure 1P**), distributed outside the intramyocardial coronary capillary network (**Figure 1Q**), and accumulated around coronary arteries (**Figure 1R**). Most of these cells were immature myeloid precursors (Mac1$^+$/Gr1$^+$), B cells (B220$^+$), and monocytes (Mac1$^+$/Gr1$^-$) (Online Figures 3D and 3F).

POST-MI VENTRICULAR REMODELING. To identify the contribution of eYFP$^+$ EPDCs to ventricular remodeling and scarring and define how such contribution is coordinated with the inflammatory process that follows MI, we transplanted irradiated *Wt1Cre*-YFP$^+$ mice with mRFP bone marrow. After reconstitution, these animals were submitted to ligation of the left anterior descending coronary artery to induce MI and ventricular remodeling was studied 1, 3, 7, 14, and 30 days after the injury (**Figure 2A**). These time points allowed for the screening of the inflammatory, proliferative, and maturation phases of MI in small mammals (6).

Left anterior descending ligation caused massive myocardial death within the first day after the damage, inducing a fast increase of circulating mRFP$^+$ BMCs to the infarct zone (IZ), whereas eYFP$^+$ EPDC density remained similar to that of the remote, noninfarcted zones (**Figure 2B**). No double mRFP$^+$/eYFP$^+$

FIGURE 1 EPDCs Pioneer Cardiac Interstitium Formation

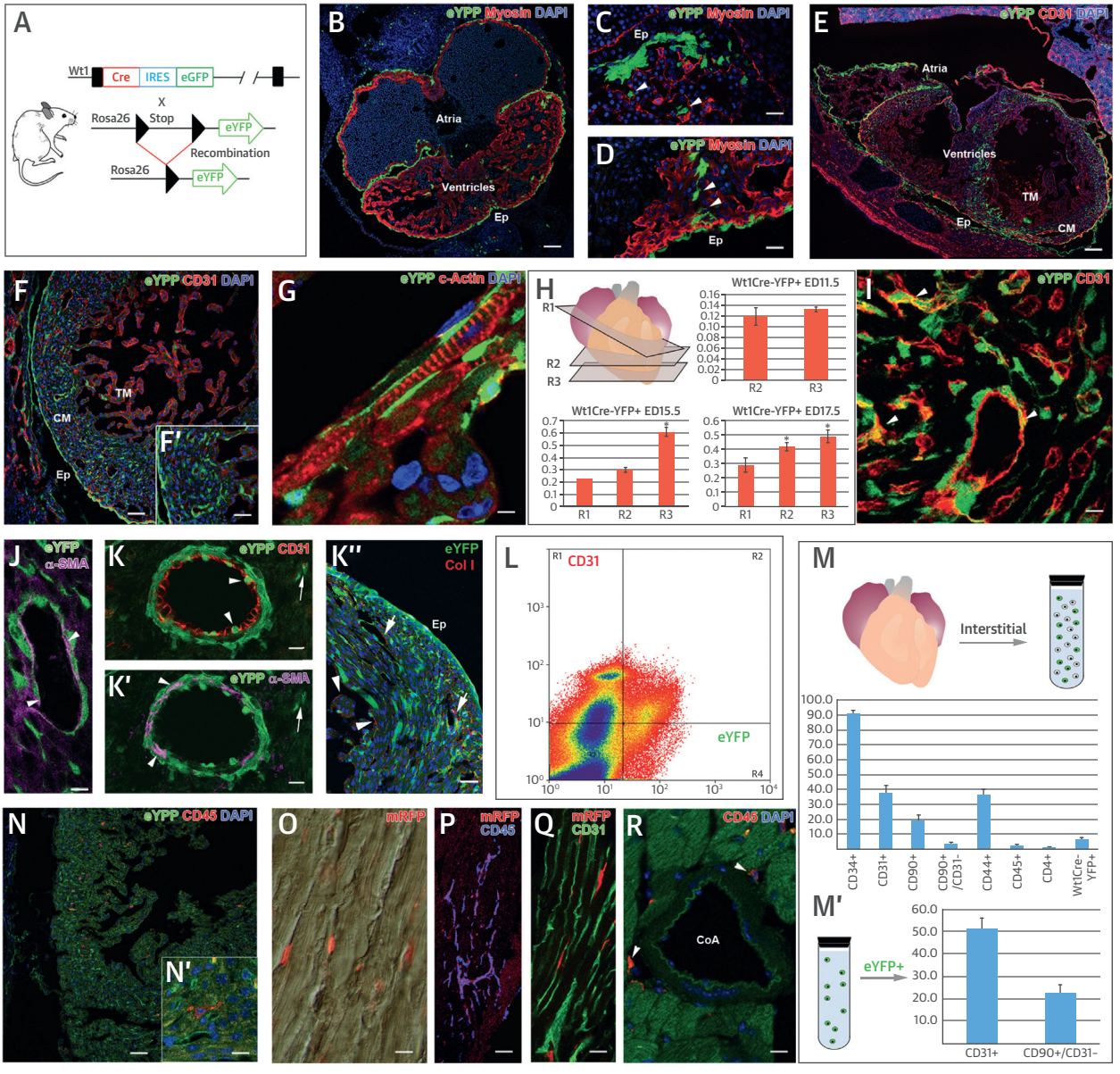

(A) Wt1Cre-YFP mice were generated with activated permanent reporter enhanced yellow fluorescent protein (eYFP+YFP$^+$) expression. **(B to D)** Epicardium (Ep) and epicardium-derived cells (EPDCs) **(arrowheads)** express YFP at embryonic day (E) 11.5. Embryonic (at E15.5 **[E]** and E17.5 **[F]**) and postnatal **(G)** eYFP$^+$ EPDCs colonize the ventricular myocardium. **(H)** The eYFP$^+$ area is normalized with respect to the total DAPI$^+$ area in different heart locations. Adult ventricular eYFP$^+$ cells integrate into coronary blood vessel endothelium **(I to K; arrowheads)**, muscular wall **(J, K, K'; arrowheads)**, or the cardiac interstitium **(K and K', arrow)**. This latter interstitial cell type does not express collagen I (Col I), present in the subendocardium **(K'', arrowheads)** or forming coronary vessels **(K'', arrows)**. **(L)** Cluster of differentiation (CD) 31$^+$ cells from adult hearts are 37% of the eYFP$^+$ interstitial population. **(M)** Interstitial cells are CD90$^+$ and CD44$^+$. FACS of total eYFP$^+$ cells identifies a putative CD90$^+$/CD31$^-$ cardiac fibroblast precursor population **(M')**. **(N and N')** CD45$^+$ cells are incorporated within the embryonic ventricular myocardium around E15.5. Transplanted adult monomeric red fluorescent protein (mRFP$^+$) bone marrow cells home at the cardiac interstitium **(O to R)**; CD45$^+$ cells **(P)** position themselves outside capillaries **(Q)**, and accumulate in the peri-coronary interstitium **(R, arrowheads)**. Scale bars: **B**, 80 μm; **C**, **D**, **I to K**, 15 μm; **E**, 150 μm; **F**, 50 μm; **F'**, **K''**, **O**, and **Q**, 30 μm; **G**, 5 μm; **N**, 60 μm; **N'** and **R**, 10 μm. CM = compact myocardium; CoA = coronary arteries; DAPI = 4',6-diamidino-2-phenylindole; eGFP = enhanced green fluorescent protein; FACS = fluorescence-activated cell sorting; α-SMA = smooth muscle actin, type α; TM = trabecular myocardium; Wt1 = Wilm's Tumor Gene 1; YFP = yellow fluorescent protein.

FIGURE 2 Post-MI Time-Dependent EPDC and BMC Cell Lineage Contribution After MI

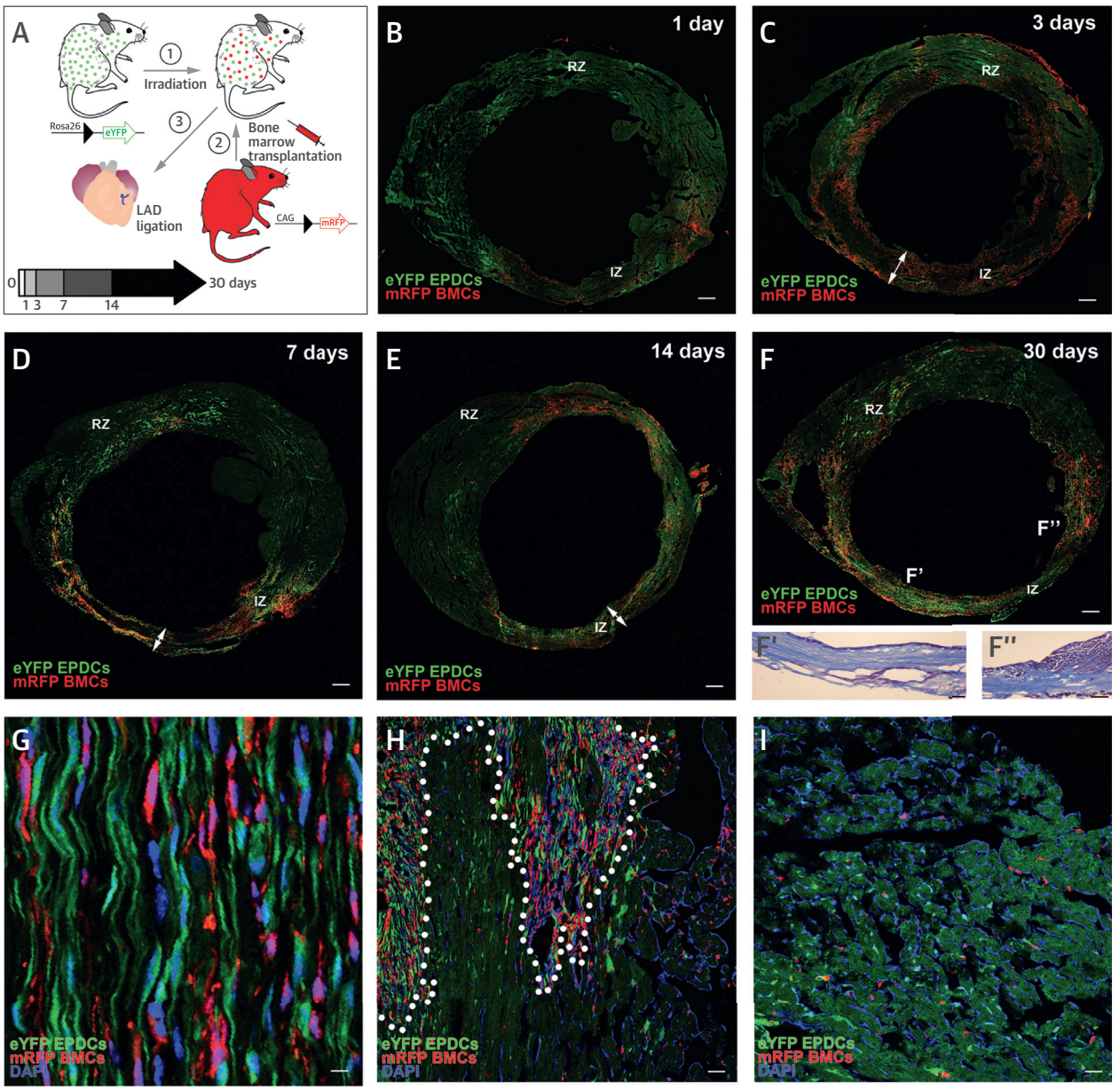

(A) *Wt1Cre*-YFP$^+$ mice were irradiated with mRFP bone marrow; after reconstitution, these mice were submitted to ligation of the left anterior descending (LAD) coronary artery to induce myocardial infarction (MI) and ventricular remodeling. Transverse sections of infarcted hearts show early mRFP$^+$ bone marrow–derived cell (BMC) infiltration, from 1 **(B)** to 3 days **(C)** post-MI. eYFP$^+$ EPDC abundance between 7 **(D)** and 14 **(E)** days after MI is shown. Thinning of the left ventricular myocardial wall is also evident **(D and E compared with C)**. By 30 days post-MI **(F)**, a full scar, mostly constituted of eYFP$^+$ fibrous tissue **(blue)**, is formed **(F', IZ; F'', BZ)**. BMCs (mRFP$^+$) and EPDCs (eYFP$^+$) accumulate together at the IZ, where they elongate and form a fibrillar mesh **(G)**; this damage-dependent accumulation is most evident at the BZ **(H, dotted line)**. The RZ presents low numbers of nonclustered, dispersed mRFP$^+$ and eYFP$^+$ cells **(I)**, equivalent to those found in normal hearts (see also Figure 1). Scale bars: **B to F**, 400 μm; **F'**, 250 μm; **F''**, 300 μm; **G**, 10 μm; **H** and **I**, 30 μm. **Double-headed arrows** in **2C to E** mark the thickness of the ventricular myocardial wall. BZ = border zone; IZ = infarct zone; RZ = remote zone; other abbreviations as in Figure 1.

cells were found at any stage analyzed, ruling out cell fusion in our experiments. Between 3 and 7 days post-MI, large numbers of cardiomyocytes were lost in the IZ and the density of eYFP$^+$ EPDCs increased in the infarct area, correlating with an evident thinning of the free left ventricular wall (from 1.48 ± 0.21 mm in control animals to 0.7 ± 0.10 mm 1 week post-MI) (Figures 2C and 2D). One week after MI, large

populations of densely packed eYFP$^+$ EPDC and mRFP$^+$ BMCs (**Figures 2E and 2F**) constituted most of the IZ tissue (**Figure 2G**), which is flanked by a border zone (BZ) containing living cardiomyocytes (**Figure 2H**). The remote zone (RZ), distant from the IZ, contained a few loosely distributed eYFP$^+$ and mRFP$^+$ cells in a pattern similar to that found in control samples (**Figure 2I**). At 14 days after MI, a deeply remodeled left ventricular wall matured into a fibrotic scar (**Figure 2E**). This condition persisted 30 days post-MI (**Figure 2F**).

CF SOURCE. Detailed histological inspection of infarcted hearts reveals characteristic spatiotemporal cellular dynamics at the IZ. One day after MI, both EPDCs and BMCs showed a random distribution (**Figure 3A**). BMCs expressed variable levels of CD45 (**Figures 3B to 3B'''**), and were the predominant cell type at the damage core (mRFP/eYFP cell ratio, 3.1 ± 0.49; mRFP/eYFP cell ratios in the BZ and RZ, 2.1 ± 0.52 and 0.3 ± 0.43, respectively). During the first day post-MI, monocytes were abundant in both systemic (not shown) and coronary blood vessels (**Figure 3C**). Monocytes extravasated from the endocardium and coronary endothelium to the underlying ventricular interstitium, which contained high numbers of eYFP$^+$ EPDCs (Online Figures 3A to 3C). A fraction of these monocytes could differentiate into the mRFP$^+$/F4/80$^+$ macrophages accumulating at the IZ (**Figure 3D**). Three days after MI, the number of EPDCs had increased with respect to BMCs (mRFP cells/eYFP cells ratio, 1.57 ± 0.26; mRFP/eYFP cell ratio, 1.7 ± 0.38 for the BZ and 0.5 ± 0.61 for the RZ), and both cell types established close contact, starting to polarize (**Figure 3E**). One week after MI, the number of EPDCs and BMCs at the IZ was similar (mRFP/eYFP cell ratio, 0.97 ± 0.18; mRFP/eYFP cell ratios in the BZ and RZ, 0.7 ± 0.22 and 0.4 ± 0.56, respectively). Both cell types were tightly packed and completely polarized, the long cell axes of EPDCs and BMCs lying in parallel. Except for some CD31$^+$ capillary endothelial cells, eYFP$^+$ EPDCs and mRFP$^+$ BMCs were 90.2 ± 2.1% of cells present at the IZ core 1 week after MI (**Figure 3F**).

FACS analysis of CD45$^+$ cells from control and infarcted hearts (7 days post-MI) confirmed a 10% decrease in B220$^+$ B cells (of total CD45$^+$ cells) and a significant increase of Mac1$^+$/Gr1$^-$ monocytes (18% of total CD45$^+$ cells) (**Figures 3G and 3H**), multipotent bone marrow (Lin$^-$/cKit$^+$/Sca1$^+$/Flk2$^+$/CD34$^+$, 34%), and megakaryocyte-erythrocyte progenitors (Lin$^-$/cKit$^+$/Sca1$^-$/FCγR^{low}/CD34$^-$, 9%) (**Figure 3H'**) in injured hearts (all these data are summarized in Online Figure 3D). Increased numbers of long-term hematopoietic stem cells (LT-HSC; cKit$^+$/Sca1$^+$/CD34$^-$/Flk2$^-$, 2%) in infarcted hearts (first week after MI) were also recorded (**Figure 3H'**). As compared with the RZ (**Figure 3I**), the IZ EPDC population mostly comprises eYFP$^+$/CD31$^-$/α-SMA^{low} fibroblasts, although some eYFP$^+$/CD31$^+$ (endothelial) and eYFP$^+$/α-SMA$^+$ (myofibroblasts) were present (**Figure 3J**). FACS analysis of eYFP$^+$ cells from infarcted hearts revealed a significant rise (45%) in the interstitial eYFP$^+$/CD31$^-$/CD90$^+$ population (**Figure 3K**).

During this period, accumulation of eYFP$^+$ EPDCs at the IZ correlated with massive extracellular collagen I protein deposition in the area (**Figure 3L**). Accordingly, data from quantitative polymerase chain reaction analysis of eYFP$^+$/CD31$^-$ cells sorted from infarcted hearts showed an increase of 3 orders of magnitude in collagen I transcription with respect to control samples. However, collagen I messenger ribonucleic acid in CD45$^+$ bone marrow derivatives was very low or undetectable at these stages (**Figure 3M**). During the third and fourth weeks after MI, the ventricular wall still hosted high numbers of BMCs (**Figures 3N and 3O**), but the cellular structure of the forming fibrotic scar remained constant: IZ mRFP/eYFP cell ratio was 0.8 ± 0.04 14 days after MI and 0.9 ± 0.08 30 days after MI. Two weeks post-MI, mRFP/eYFP cell ratios were 0.8 ± 0.49 for the BZ and 0.5 ± 0.37 for the RZ; 4 weeks after MI, the BZ and RZ mRFP/eYFP ratios were 0.7 ± 0.36 and 0.4 ± 0.74, respectively. Massive extracellular deposition of collagen I fibers, arranged in parallel to the major axis of elongated eYFP$^+$ EPDCs, and progressive decellularization of the IZ were evident in this phase (**Figure 3P**), in which proinflammatory cytokine (interleukin-6, tumor necrosis factor-α) accumulation overlapped with BMCs (Online Figures 3E and 3F). Both multipotent bone marrow progenitors and LT-HSCs significantly decreased between 7 and 30 days after MI. However, whereas multipotent bone marrow progenitors fell to levels similar to that of control animals, LT-HSC numbers remained significantly elevated with respect to control animals 1 month after MI (Online Figures 3G and 3H). Total changes in BMC/EPDC ratios (during 1 month after MI) are shown in **Figure 3Q**.

To further confirm that Wt1-eYFP$^+$ CFs in the infarcted heart differentiated from resident interstitial cells and not from adult epicardial epithelial to mesenchymal transition reactivation, we checked the expression of epicardial markers, such as Wt1, cytokeratins, and Raldh2, in the eYFP$^+$ subepicardium of infarcted hearts. As shown in Online Figures 3I to 3K, no significant expression of these markers could be traced from the epicardium to

FIGURE 3 Epicardium-Derived CFs Build up Infarction Scar

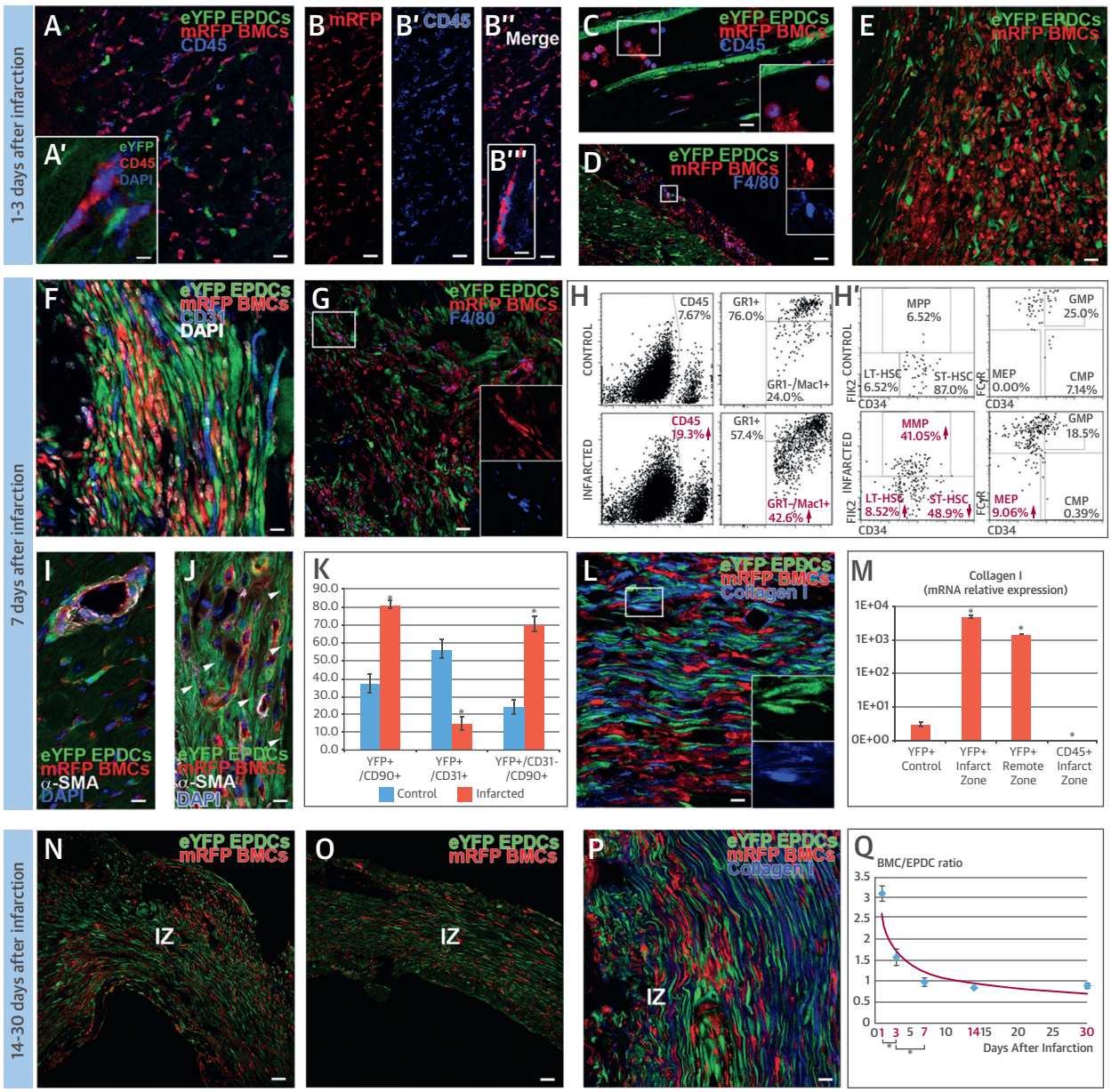

(A) eYFP$^+$ EPDCs and mRFP$^+$ BMCs shown at the IZ 1 day after MI. **(A', B, B', B'', B''')** Most mRFP$^+$ BMCs are CD45$^+$, including monocytes **(C)** and macrophages **(D)**. **(E)** Early polarization of RFP$^+$ and YFP$^+$ cells (3 days post-MI) becomes evident 7 days after MI **(F)**. CD31 staining shows that BMCs are not circulating **(F)**; some BMCs are F4/80$^+$ macrophages **(G)**. FACS of CD45$^+$ cells sorted from infarcted and control hearts shows a rise in Mac1$^+$/Gr1$^-$ monocytes after MI **(H)**. FACS analysis of the cKit$^+$/Sca1$^+$ fraction identifies cardiac Flk2$^+$/CD34$^+$ multipotent bone marrow progenitors, FCγR^{low}/CD34$^-$ megakaryocyte-erythrocyte progenitor, and CD34$^-$/Flk2$^-$ LT-HSCs after MI **(H', red = significant changes)**. Seven days after MI, IZ EPDCs, but not RZ EPDCs, equal BMCs **(I compared with J)**. IZ EPDCs are eYFP$^+$/CD31$^-$/α-SMA^{low} **(J, arrowheads)** and CD90$^+$ **(K)**. Up-regulation of extracellular and intracellular collagen **(L)** is confirmed by Col I mRNA increase in EPDCs, but not BMCs, after MI **(M)**. IZ BMC/EPDC packing is maintained 14 **(N)** and 30 **(O)** days after MI, and Col I deposition precedes decellularization of the IZ **(P)**. **(Q)** Post-MI BMC/EPDC changes were significant early, between 2 time periods within the first week, but relatively flat for the rest of the month. *$p < 0.05$. Scale bars: **A to C**, **E**, and **L**, 15 μm; **B'''** and **F**, 10 μm; **I** and **J**, 5 μm; **N** and **O**, 90 μm; **P**, 12 μm; **A'**, 2.5 μm. CF = cardiac fibroblast; LT-HSC = long-term hematopoietic stem cell; MEP = megakaryocyte-erythroid progenitor; MPP = multipotent hematopoietic progenitor; mRNA = messenger ribonucleic acid; ST-HSC = short-term hematopoietic stem cell; other abbreviations as in Figures 1 and 2.

the subepicardium at any stage studied (3 to 7 days post-MI).

EPDC CONTRIBUTION TO CF. Because recent reports have separately involved epicardial (18) and bone marrow derivatives (19) in nonischemic fibrosis, we decided to evaluate eYFP$^+$ EPDC contribution to cardiac fibrosis in this context. We thus induced hypertension in *Wt1Cre*-eYFP$^+$ mice via angiotensin II subcutaneous infusion. Surprisingly, this treatment yielded a low number of epicardial-derived (eYFP$^+$) CFs to hypertensive heart fibrosis (Online Figures 4A to 4C), a finding that differs from those reported after transaortic constriction-induced pressure overload, which showed a significant epicardial contribution to CF (20,21).

One week after MI, cKit$^+$ (CD117$^+$) mRFP$^+$ BMCs were found embedded in the eYFP$^+$ EPDC-rich tissue of the IZ and BZ, often in association with coronary blood vessel walls (Figure 4A). FACS comparison of CD45$^+$ cells isolated from infarcted (7 and 30 days after MI) and stage-matched control tissue samples confirmed the increase in bone marrow-derived cKit$^+$ progenitors and primitive HSCs (Lin$^-$/Sca1$^+$/cKit$^+$) in the experimental group, and their subsequent decrease 1 month after MI (Figure 4B). Prompted by the characteristic association between cKit$^+$ BMCs and eYFP$^+$ EPDCs, we investigated BMC-EPDC interaction in vitro. Coculture of mononuclear enhanced green fluorescent protein bone marrow cells and a continuous embryonic epicardial cell line (EPIC) (22), revealed the preferential attachment of enhanced green fluorescent protein mononuclear BMCs to EPIC (23.11 ± 3.5% of total cultured cells) when compared with mononuclear BMC-tracheal smooth muscle cells cocultures (3.9%

FIGURE 4 Bone Marrow Progenitor Profiles, Cell Proliferation, and Recruitment

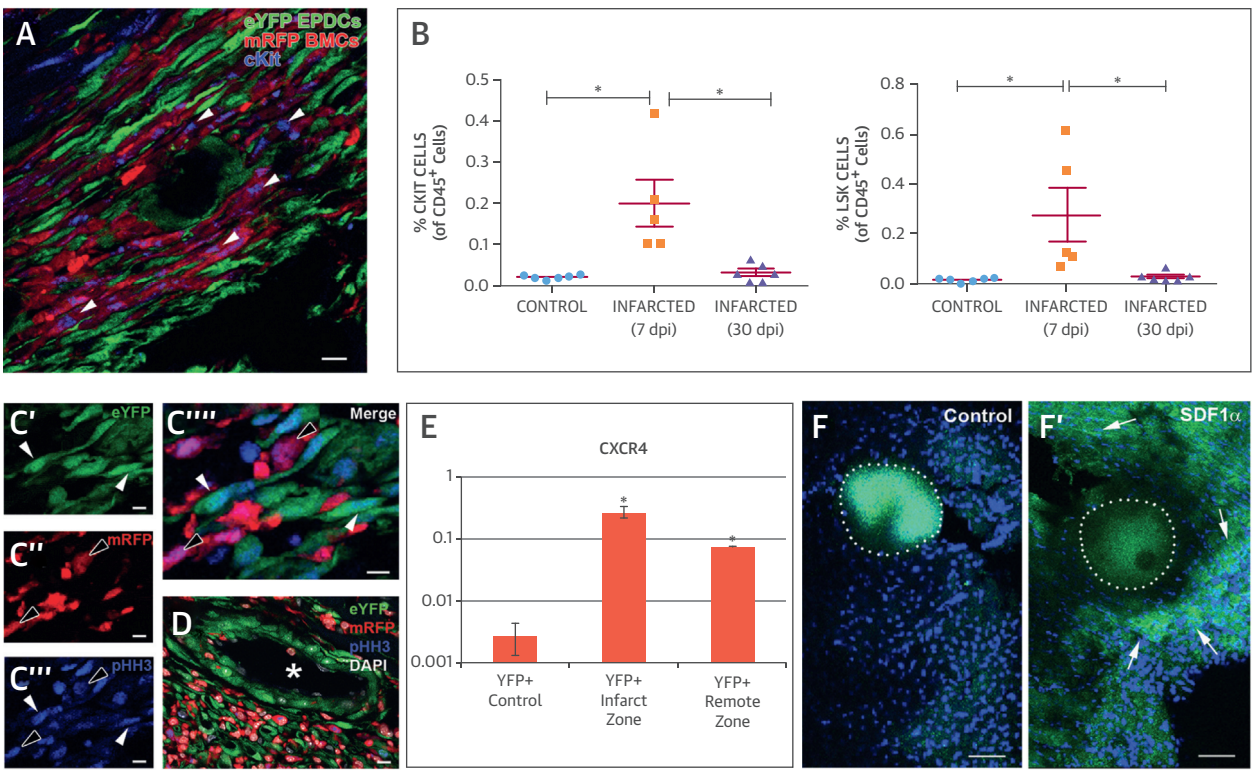

(A) From 7 days post-MI onward, cKit$^+$ cells accumulated at the infarct site and around BZ coronary vessels **(arrowheads)**. **(B)** cKit$^+$ and the most primitive hematopoietic stem cells (Lin$^-$/Sca1$^+$/cKit$^+$, [LSK]) significantly increase in the Lin$^-$/CD45$^+$ fraction post-MI. Proliferating cells at the IZ-BZ interface **(C' through C'''')** are both mRFP$^+$ BMCs **(black arrowheads)** and eYFP$^+$ EPDCs **(white arrowheads)**, and remain close to coronary blood vessels **(D, asterisk)**. EPDCs increase *CXCR4* transcription levels **(E)** and respond to a stromal cell-derived factor 1α (SDF-1α) chemokine trap **(F, dotted line)**, accumulating over its surface **(F', arrows)**. Scale bars: **A**, 15 μm; **C-C'''**, 5 μm; **C''''**, 10 μm; **F** and **F'**, 30 μm. **Asterisks** in **4B** and **4E** indicate statistically significant differences ($p < 0.05$). pHH3 = phosphohistone H3; other abbreviations as in Figures 1 and 2.

CENTRAL ILLUSTRATION **Origin of Fibroblasts in the Infarcted Heart**

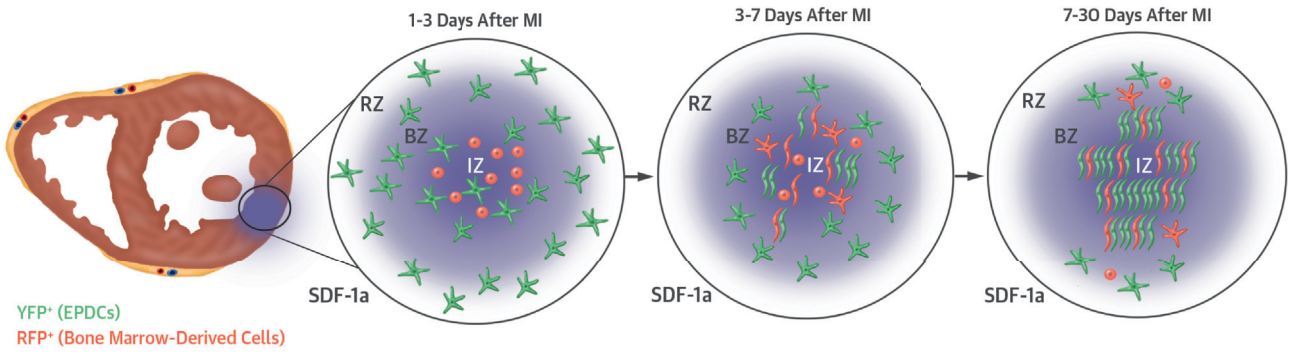

Ruiz-Villalba, A. et al. J Am Coll Cardiol. 2015; 65(19):2057–66.

This illustration depicts the interaction and spatial arrangement of epicardium-derived cells (EPDC) **(green)** and bone marrow–derived cells **(orange)** as they build up post-myocardial infarction (MI) scar, expanding from the central infarct zone (IZ) to the adjacent border zone (BZ). The chemotactic stromal cell–derived factor (SDF)-1α gradient is shown in **blue**. RFP = red fluorescent protein; RZ = remote zone; YFP = yellow fluorescent protein.

± 0.75 of total cultured cells; $p < 0.05$) (Online Figures 5A to 5D).

Phosphohistone H3 immunohistochemistry in our samples identified mitotic cells in both mRFP$^+$ BMC and eYFP$^+$ EPDCs between the IZ and BZ compartments (**Figures 4C′ to C‴′ and 4D**). To test whether chemotaxis could be involved in eYFP$^+$ EPDC accumulation at the IZ, we isolated eYFP$^+$ EPDCs from control and infarcted hearts and found that CXCR4 messenger ribonucleic acid transcription in eYFP$^+$ cells was increased by 2 orders of magnitude in infarcted hearts (**Figure 4E**). To confirm that eYFP$^+$ EPDCs can respond to SDF-1α signals, patterned SDF-1α delivery to Wt1Cre-YFP heart walls was carried out. Accumulation of eYFP$^+$ EPDC around the SDF-1α source confirmed a robust migratory response of these cells toward this chemokine (**Figures 4F and F′**).

DISCUSSION

In this study we aimed to identify the origin of CFs in the infarcted heart (**Central Illustration**). Our genetic cell-tagging strategy allowed us to trace epicardial-derived mesenchymal cells (*Wt1*Cre-eYFP$^+$) from the embryonic to the adult cardiac interstitium and identify the eYFP$^+$/CD31$^-$/CD90$^+$ cell fraction as the major source of CF after MI. Although CF differentiation from epicardial epithelial to mesenchymal reactivation after MI cannot be ruled out (10), our data indicate that this is not the main mechanism responsible for the expansion of epicardial-derived CFs in the ischemic heart, which seems to take place by proliferation and local recruitment of eYFP$^+$/CD31$^-$/CD90$^+$ cells via the myocardially secreted chemokine SDF-1α (23). The reported changes in the BMC/EPDC ratio (falling from 3.1 to 0.97 at 1 week after MI) illustrate the cellular dynamics of the remodeling ventricle and clearly show that the massive increase of EPDCs in the IZ follows the recruitment of BMCs to the damage site.

We have also provided data showing that BMC contribution to the CF population after MI is a minor one. However, we suggest that BMC-EPDC interaction is involved in triggering the critical transition from reparative fibrosis to malignant scarring in the infarcted heart. All these results, which are in accord with the genetic expression profile of the cardiac interstitium after MI (15), do not necessarily argue against the reported differentiation of circulating cells (24) or endothelial cells (25) into CFs, but point to the necessity of compared collagen synthesis quantification to establish the specific contribution of defined cell populations to the building of the extracellular matrix in ischemic and nonischemic cardiac fibrosis.

STUDY LIMITATIONS. Our study is limited by the technical restrictions of multiple cell lineage tracing, because it is very difficult to label more than 2 cell types at the same time, but also by the challenging histological identification of some specific hematopoietic cell surface markers. Further research is needed to identify all the cell types participating in ventricular remodeling and scarring after MI.

CONCLUSIONS

Our work unambiguously shows that the epicardial-derived interstitial cell population includes a pool of fibroblast precursors ($CD90^+/CD31^-/\alpha\text{-}SMA^{low/-}$) that massively differentiate into CFs ($CD90^+/CD31^-/\alpha\text{-}SMA^{low}$) after MI. We have thus identified the epicardium as the main source of CFs in the ischemic heart. Moreover, our data indicate that EPDC-BMC interaction provides the cellular scaffolding required for patterned collagen deposition in the post-MI fibrotic scar. We believe that the manipulation of this cellular interaction could help to minimize cardiac fibrosis and improve cell-based therapies to repair the infarcted heart.

ACKNOWLEDGMENTS The authors thank Dr. J.B. Burch (National Institutes of Health, Bethesda, Maryland) for the Wt1Cre line, Dr. E. Manjón-Cabeza (University of Málaga, Spain) for her help on graphic design, and D. Navas for his support on confocal microscopy.

REPRINT REQUESTS AND CORRESPONDENCE: Dr. José M. Pérez-Pomares, Department of Animal Biology, Faculty of Sciences, University of Málaga, Campus de Teatinos s/n, Málaga 29071, Spain. E-mail: jmperezp@uma.es.

PERSPECTIVES

COMPETENCY IN MEDICAL KNOWLEDGE: Fibrosis is a hallmark of post-infarction ventricular remodeling, but most therapies fail to control fibrosis.

TRANSLATIONAL OUTLOOK: Recognition that most cardiac fibroblasts in the ischemic heart originate in the epicardium may stimulate research to identify pharmacological targets that inhibit myocardial fibrosis among survivors of myocardial infarction.

REFERENCES

1. Mozaffarian D, Benjamin EJ, Go AS, et al. Executive summary: heart disease and stroke statistics – 2015 update: a report from the American Heart Association. Circulation 2015;131:434–41.

2. Laflamme MA, Murry CE. Heart regeneration. Nature 2011;473:326–35.

3. Couzin-Frankel J. The elusive heart fix. Science 2014;345:252–7.

4. Jessup M, Brozena S. Heart failure. N Engl J Med 2003;348:2007–18.

5. Daskalopoulos EP, Janssen BJA, Blankesteijn WM. Myofibroblasts in the infarct area: concepts and challenges. Microsc Microanal 2012;18:35–49.

6. Dobaczewski M, Gonzalez-Quesada C, Frangogiannis NG. The extracellular matrix as a modulator of the inflammatory and reparative response following myocardial infarction. J Mol Cell Cardiol 2010;48:504–11.

7. González A, Ravassa S, Beaumont J, López B, Díez J. New targets to treat the structural remodeling of the myocardium. J Am Coll Cardiol 2011;58:1833–43.

8. De Bakker JM, van Capelle FJ, Janse MJ, et al. Fractionated electrograms in dilated cardiomyopathy: origin and relation to abnormal conduction. J Am Coll Cardiol 1996;27:1071–8.

9. Spach S, Boineau J. Microfibrosis produces electrical load variations due to loss of side-to-side cell connections: a major mechanism of structural heart disease arrhythmias. Pacing Clin Electrophysiol 1997;20:397–413.

10. Zeisberg E, Kalluri R. Origins of cardiac fibroblasts. Circ Res 2011;107:1304–12.

11. Aranguren XL, McCue JD, Hendrickx B, et al. Multipotent adult progenitor cells sustain function of ischemic limbs in mice. J Clin Invest 2008;118:504–14.

12. Pérez-Pomares JM, Macías D, García-Garrido L, Muñoz-Chápuli R. Contribution of the primitive epicardium to the subepicardial mesenchyme in hamster and chick embryos. Dev Dyn 1997;210:96–105.

13. Pérez-Pomares JM, Macías D, García-Garrido L, Muñoz-Chápuli R. The origin of the subepicardial mesenchyme in the avian embryo: an immunohistochemical and quail-chick chimera study. Dev Biol 1998;200:57–68.

14. Gittenberger-de Groot A, Vrancken Peeters MP, Mentink MM, Gourdie RG, Poelmann RE. Epicardium-derived cells contribute a novel population to the myocardial wall and the atrioventricular cushions. Circ Res 1998;82:1043–52.

15. Furtado MB, Costa MW, Pranoto EA, et al. Cardiogenic genes expressed in cardiac fibroblasts contribute to heart development and repair. Circ Res 2014;114:1422–34.

16. Carlson S, Trial J, Soeller C, Entman ML. Cardiac mesenchymal stem cells contribute to scar formation after myocardial infarction. Cardiovasc Res 2011;91:99–107.

17. Van de Pavert SA, Ferreira M, Domingues RG, et al. Maternal retinoids control type 3 innate lymphoid cells and set the offspring immunity. Nature 2014;508:123–7.

18. Chong JJH, Chandrakanthan V, Xaymardan M, et al. Adult cardiac-resident MSC-like stem cells with a proepicardial origin. Cell Stem Cell 2011;9:527–40.

19. Haudek SB, Xia Y, Huebener P, et al. Bone marrow-derived fibroblast precursors mediate ischemic cardiomyopathy in mice. Proc Natl Acad Sci U S A 2006;103:18284–9.

20. Ali SR, Ranjbarvaziri S, Talkhabi M, et al. Developmental heterogeneity of cardiac fibroblasts does not predict pathological proliferation and activation. Circ Res 2014;115:625–35.

21. Moore-Morris T, Guimarães-Gamboa N, Banerjee I, et al. Resident fibroblast lineages mediate pressure overload-induced cardiac fibrosis. J Clin Invest 2014;124:2921–34.

22. Ruiz-Villalba A, Ziogas A, Ehrbar M, Pérez-Pomares JM. Characterization of epicardial-derived cardiac interstitial cells: differentiation and mobilization of heart fibroblast progenitors. PLoS One 2013;8:e53694.

23. Castellani C, Padalino M, China P, et al. Bone-marrow-derived CXCR4-positive tissue-committed stem cell recruitment in human right ventricular remodeling. Hum Pathol 2010;41:1566–76.

24. Haudek SB, Cheng J, Du J, et al. Monocytic fibroblast precursors mediate fibrosis in angiotensin-II-induced cardiac hypertrophy. J Moll Cell Cardio 2010;49:499–507.

25. Weisberg EM, Tarnavski O, Zeisberg M, et al. Endothelial-to-mesenchymal transition contributes to cardiac fibrosis. Nat Med 2007;13:952–61.

KEY WORDS cardiomyocyte, cell therapy, fibrosis, hematopoietic progenitor, ischemia

APPENDIX For supplemental tables and figures, please see the online version of this article.